HHS Public Access

Author manuscript

Urolithiasis. Author manuscript; available in PMC 2017 December 01.

Published in final edited form as:

Urolithiasis. 2017 October ; 45(5): 507–513. doi:10.1007/s00240-016-0959-5.

Development of a Novel Magnetic Resonance Imaging Acquisition and Analysis Workflow for the Quantification of Shock Wave Lithotripsy-Induced Renal Hemorrhagic Injury

Rajash K. Handa[1], **Paul R. Territo**[2], **Philip M. Blomgren**[1], **Scott A. Persohn**[2], **Chen Lin**[2], **Cynthia D. Johnson**[1], **Lei Jiang**[2], **Bret A. Connors**[1], and **Gary D. Hutchins**[2]

[1]Department of Anatomy and Cell Biology (RKH, PMB, CDJ, BAC), Indiana University School of Medicine, Indianapolis, IN, USA

[2]Department of Radiology and Imaging Sciences (PRT, SAP, CL, LJ, GDH), Indiana University School of Medicine, Indianapolis, IN, USA

Abstract

Introduction—The current accepted standard for quantifying shock wave lithotripsy (SWL)-induced tissue damage is based on morphometric detection of renal hemorrhage in serial tissue sections from fixed kidneys. This methodology is time and labor intensive and is tissue destructive. We have developed a non-destructive magnetic resonance imaging (MRI) method that permits rapid assessment of SWL-induced hemorrhagic lesion volumes in post-mortem kidneys using native tissue contrast to reduce cycle time.

Methods—Kidneys of anesthetized pigs were targeted with shock waves using the Dornier Compact S lithotripter. Harvested kidneys were then prepared for tissue injury quantification. T1 weighted (T1W) and T2 weighted (T2W) images were acquired on a Siemens 3T Tim Trio MRI scanner. Images were co-registered, normalized, difference (T1W–T2W) images generated, and volumes classified and segmented using a Multi-Spectral Neural Network (MSNN) classifier. Kidneys were then subjected to standard morphometric analysis for measurement of lesion volumes.

Results—Classifications of T1W, T2W and difference image volumes were correlated with morphometric measurements of whole kidney and parenchymal lesion volumes. From these relationships, a mathematical model was developed that allowed predictions of the morphological parenchymal lesion volume from MRI whole kidney lesion volumes. Predictions and morphology were highly correlated (R=0.9691, n=20) and described by the relationship y=0.84x+0.09, and highly accurate with a sum of squares difference error of 0.79%.

Conclusions—MRI and the MSNN classifier provide a semi-automated segmentation approach, which provide a rapid and reliable means to quantify renal injury lesion volumes due to SWL.

Contact Information: Rajash K. Handa, Ph.D. rajash_handa@hotmail.com.

Conflict of interest Authors RKH, PRT, SAP, CL, CDJ, LJ, BAC and GDH declare no conflict of interest.

Ethical approval All applicable international, national, and/or institutional guidelines for the care and use of animals were followed.

Keywords

magnetic resonance imaging; kidney; shock wave lithotripsy; tissue injury

Introduction

Shock wave lithotripsy (SWL) is a commonly used noninvasive treatment modality for uncomplicated renal and ureteral stones [1]. Although effective in breaking stones, SWL can produce undesirable side effects in the kidney resulting in tissue injury [2,3]. The primary acute lesion is trauma to blood vessels with extra-vasculature pooling of blood within the renal tissue. Tissue damage from SWL also extends to the tubules and glomeruli [2,3], and the production and release of inflammatory and oxidative stress mediators [4,5], which can result in fibrosis and loss of functional tissue [2,6,7]. Such injury from SWL has been linked to adverse patient outcomes, e.g. hypertension and exacerbation of kidney stone disease [8,9]. Consequently, therapeutic strategies are being developed to minimize tissue injury and shorten recovery times to mitigate possible SWL treatment complications [1,6,10,11].

The current accepted standard (i.e. “gold standard”) method for quantifying the acute tissue injury response to SWL treatments is based on morphometric detection of hemorrhage in serial tissue section images captured with a high-quality digital camera from fixed latex-perfused kidneys [12]. This approach is time and labor intensive, requires expert knowledge of renal anatomy and image processing to generate accurate results. Moreover, because this method requires serial sectioning of dehydrated tissues and photographic image capture, it is inherently destructive, thus limiting subsequent tissue level analysis of the affected organ. To hasten improvements in SWL safety, there is a need to develop rapid and noninvasive methods for quantifying the tissue injury response to SWL treatment strategies. One approach is the use of plasma and urinary biomarkers of tissue injury, which have been assessed in renal SWL research and yielded mixed results [13,14]. Little is known on whether such biomarkers are correlated to any direct measurement of lithotripsy-induced renal damage [15]. Our approach is to develop a rapid and noninvasive method for quantifying SWL-induced hemorrhagic lesions that can be translated to human use. As a first step in achieving this objective, we report the development of a novel magnetic resonance imaging (MRI) acquisition and analysis workflow, which permits rapid assessment of hemorrhagic lesions in *ex-vivo* kidneys using native tissue contrast to reduce cycle time whilst maintaining the information on lesion volumes.

Methods

All animal studies were conducted in accordance with the National Institutes of Health Guide for the Care and Use of Laboratory Animals and were approved by the Institutional Animal Care and Use Committee of Indiana University School of Medicine.

Quantification of the hemorrhagic lesion in *ex-vivo* kidneys

***In vivo* experiments—**Adult female farm pigs were prepared for SWL as previously described [16]. In brief, pigs were anesthetised (induction with 20 mg/kg ketamine and 2

mg/kg xylazine; maintenance with 1–3% isoflurane) and catheters were placed in the femoral artery and ureters for blood pressure monitoring and urine collection, respectively. The urinary collecting system of the left kidney was identified with intra-ureteral administration of contrast agent and X-ray fluoroscopy. The lower pole of one kidney was then targeted with SWs using the Dornier Compact S lithotripter, where the SW number (2500 SWs), rate (60 – 120 SWs/min) and power level (PL 3 – 6) was varied to yield a wide range of hemorrhagic lesion volumes.

***Ex vivo* imaging—**Following SWL and at the time of euthanasia, kidneys were perfused fixed *in situ* with 2.5% glutaraldehyde in 0.1 M cacodylate buffer (pH 7.4) followed by organ resection [12,16]. Post fixation, T1 weighted (T1W) 3D-FLASH (120mm FOV, 0.5mm Slice thickness, 0.3×0.3mm spatial resolution, 384 Base resolution, 5.32ms TR, 2.05ms TE, 4 Averages, 128 slices, 12 Degree Flip angle, no FS) and T2 weighted (T2W) 3D-SPACE (120mm FOV, 0.5mm Slice thickness, 0.3×0.3mm spatial resolution, 384 Base resolution, 2000ms TR, 190ms TE, 1.4 Averages, 128 slices, T2 variable Flip angle (i.e. Flip angle of refocusing pulse varies across the echo train), no FS) images were acquired on a Siemens 3T Tim Trio MRI scanner using a high sensitivity 72mm inner diameter 8 channel coil (RapidMR).

Morphological Analysis—After MRI, the fixed *ex-vivo* kidneys were injected with latex (Microfil®) to fill the microvasculature; sequentially dehydrated through graded ethanol (30%, 50%, 70%, 95%, 100%) and chloroform (100%) solutions; embedded in paraffin; serially sectioned in the transverse plane every 40 μm, with digital photographs taken every 120 μm [12]. Digital images were imported into Photoshop and the lesion volume determined by interpolating between digital sections, where the final volume was expressed as a percentage of the whole kidney volume and/or parenchymal functional volume [12].

MRI Analysis—To provide image segmentation of hemorrhagic lesions, T1W and T2W DICOM images were imported in to Analyze 12.0 (AnalyzeDirect), spatially registered according to the methods of Studholme et al [17], intensity normalized over the interval [0.0, 1.0], and difference image constructed (i.e. T1W–T2W). To train the multi-spectral neural network classifier (MSNN), regions of interest for normal kidney (cortex and medulla), hemorrhagic lesions (bright on T1W, dark on T2W), and background (image space outside the kidney) were defined manually and stored. The regions were then applied to the registered normalized T1W (R-N-T1W), T2W (R-N-T2W), and T1W-T2W images and back-propagated to define the MSNN model weights to permit voxel-wise classification. Using the predefined weights from the training image sets, all subsequent images were processed as defined in Figure 1 thus yielding 3D object maps for normal kidney tissue, hemorrhagic lesion, and background. Object maps were then quantified for region volumes according to the following general equation:

$$V(i)=\sum_{j=1}^{a}\sum_{k=1}^{b}\sum_{l=1}^{c} o_{Map}(i,j,k,l) * \mu(j,k,l) \quad (1)$$

Where V, i, j, k, l, a, b, c, O_{Map}, and μ are the volume of the "*i'th*" region, "*j'th*" object map index, "*k'th*" object map index, "*l'th*" object map index, "*a*" total number of row voxels, "*b*" total number of column voxels, "*c*" total number of slices, object map, and voxel dimension in millimeters.

To account for differences in apparent volumes caused by the preparations (i.e. morphological vs. MRI), percent lesion for both methods were computed as follows:

$$L(i)=\frac{V_L(i)}{V_N(i)*V_P(i)}*100 \quad (2)$$

Where L, i, V_N, V_P, and V_L are the percentage of the lesion volume, the "*i'th*" subject, the total normal volume, total parenchymal volume, and the total lesion volume, respectively.

Statistical Analysis—Analysis of lesion percentages between the morphological and MRI methods was compared using Pearson-Product Correlation Analysis (SigmaPlot 12.5). To estimate the prediction error between MRI modeled parenchymal volumes and those derived from the morphological approach, the sum of squared difference (SOSD) was computed as follows:

$$SOSD=\sum_{i=1}^{n}(L_{Morph}(i)-L_{MRI}(i))^2 \quad (3)$$

Where i, n, L_{Morph} and L_{MRI} are the "*i'th*" subject, the total subjects, kidney lesion via morphology according to Blomgren et al [12], and the kidney lesion via MRI.

Results

Quantification of the hemorrhagic lesion in *ex-vivo* kidneys

Due to the intrinsic relaxivity of water protons, SWL-induced hemorrhagic lesions appear hyper-and hypo-intense on T1 weighted (T1W) and T2 weighted (T2W) MR images, respectively. Due to the opposite magnitude for lesions in both T1W and T2W images, when difference images are constructed from registered and normalized (i.e. [0,1.0]) images, the resultant image, which is bound over the interval [−1.0, 1.0], minimizes the normal tissue contrast and accentuates the hemorrhagic lesion as hyper-intense. Importantly, using the workflow described in Figure 1, hemorrhagic lesion distributions closely match that in the morphological image (Figure 2). Since standard segmentation schemes (i.e. thresholding, region growing, and object recognition) failed to yield satisfactory lesion classification, an alternative approach was employed using a Multi-Spectral Neural Network (MSNN) classifier (Figure 3). Normalized T1W, T2W and difference (T1W–T2W) images from a single well defined case served as model inputs (Figure 3), where classes (i.e. regions) were defined for background, hemorrhagic lesion, and normal kidney, and input weights were initialized with normally distributed random values. The model was then run for 200 epochs, with 15 hidden layers (5 per class), a 0.1 minimum and alpha probability of 0.1 and 0.25,

respectively. The computed output weights were then used to modify the input weights by back propagation of error terms from the training images, and all weights and classes were then applied to all subsequent analyses. Using this approach, comparisons of whole kidney hemorrhagic lesion were highly correlated between morphology and MRI assessments (Figure 4, panel A), with an R of 0.98 (n = 10, $p<0.001$), and can be described by the relationship: $y = 0.36x + 0.13$, where the lesions ranged broadly for morphology (x = 0 – 7.7%) and MRI (y = 0 – 2.7%).

To determine the impact of the SWL-induced lesion on parenchymal (functional tissue) kidney volumes, image segmentation by MSNN classification was performed on the same MR images; however, post-segmentation hemorrhagic lesions which extended into the renal sinus were manually reassigned to normal (i.e. non-lesion) classes by a trained analyst. These data were similarly correlated between morphology and MRI (Figure 4, panel B), with an R of 0.97 (n = 10, $p<0.001$), and can be described by the relationship: $y = 0.74x + 0.002$, where the lesions ranged broadly for morphology (x = 0 – 3.3%) and MRI (y = 0 – 2.6%). From this, a mathematical model was developed that permitted predictions of morphological parenchymal lesions from MRI whole kidney lesion volumes. Figure 4, panel C shows data points of the predicted morphological parenchymal lesions from MRI whole kidney lesion volumes and the measured morphological parenchymal lesion volume. Predictions and morphology were highly correlated with an R of 0.9648 (n = 20, $P<0.001$) and described by the relationship $y = 0.84x + 0.09$. The quantification of the hemorrhagic lesion by MRI was highly accurate with a SOSD error of 0.79% between prediction and morphology estimates. The mean values of measured morphological and MRI-modeled morphological estimates of parenchymal lesions were statistically similar when the data was stratified according to the volume of the measured morphological lesion (Figure 4, panel D). Comparison of the two methods for estimating minimal (0 – 0.1%), modest (0.11 – 1%) and larger (1.1 – 4%) parenchymal lesion volumes had P values of 0.1302 (n=10), 0.6172 (n=5) and 0.2317 (n=5), respectively.

Discussion

The present report describes the development of a novel MRI acquisition and analysis workflow, which permits rapid assessment of hemorrhagic lesion volumes in *ex-vivo* kidneys using native tissue contrast. Normalized T1W, T2W and difference (T1W–T2W) images were subjected to MSNN classification to identify normal, lesion and background regions in the image. The data was highly correlated between MRI and morphological assessment of the hemorrhagic lesion in the entire kidney and we refined the technique to include functional parenchymal tissue volumes. From these relationships, a mathematical model was developed that allowed the prediction of morphological parenchymal lesions from MRI whole kidney lesion volumes. The mathematical model was highly accurate with a SOSD error of 0.79% between predictions and morphological assessment of the parenchymal hemorrhagic lesion.

Advantages of the MRI work flow method for quantification of tissue hemorrhagic lesions is that it is largely automated and does not require the user to have expert knowledge of renal anatomy; it is non-destructive and therefore tissue can be used for additional investigation;

analysis is rapid requiring ~2 hours of image capture and processing to obtain the lesion volume making the method highly cost-effective (~$400 per kidney). In contrast, the current accepted method ("gold standard") for quantification of SWL-induced hemorrhagic lesions involves embedding a kidney for serially sectioning, recording and digitization of camera captured images. Intra-parenchymal hemorrhagic volume is then estimated by manually outlining the sinus region and areas of hemorrhagic within the parenchyma in each tissue section (about 200 tissue sections per kidney) assisted with computer color recognition software (Photoshop, Adobe) [12]. This morphological based procedure is labor intensive and time consuming taking several weeks to analyze a single damaged kidney with associated costs being at least six-fold greater than the MRI approach. Both MRI and morphological methods require adequate vascular perfusion of the kidney to remove blood from normal microvessels and thereby improve the accuracy of segmentation. However, there are several additional critical steps for success of the morphological analysis procedure that include: adequate fixation of the tissue; adequate vascular perfusion with latex to enhance the contrast between kidney lesion, parenchyma and renal sinus; obtaining well-defined digital images during serial sectioning of the kidney; and the user must have expert knowledge of renal anatomy and specialized software for image processing.

As part of the development of the MRI method for tissue hemorrhagic quantification, segmentation of the parenchyma in MR images was done and revealed that the measured parenchymal hemorrhagic volume by MRI was about 74% of that estimated by the morphological method. The reason(s) for the two different estimates of the parenchymal hemorrhagic volume is unknown; although it is clear that MRI has an in plane spatial resolution (0.3mm) 6 fold lower than the morphological approach (0.05mm). This difference in spatial resolution and the apparent partial volume effects encountered with MRI may lead to possible underestimation of lesion volumes when lesions are below the scan resolution. By contrast, the morphological method [12] involves significant dehydration and shrinkage of the kidney to about 30% of its normal size and the effect of this tissue-processing step on hemorrhage sites, i.e. lesion volumes, is unknown. Regardless, modeling of the MRI data allows a high degree of accuracy between MRI-based predictions and morphologic estimates of parenchymal lesion volumes. Furthermore, there is a strong positive linear relationship between MRI prediction and morphologic estimates of parenchymal hemorrhagic lesion volumes, which allows MRI assessment of stone treatment strategies that may reduce or increase renal tissue injury. The mathematical formulae used in the MRI estimation of the morphological parenchymal hemorrhagic volume can also be easily scaled for kidney size (i.e. animals of different ages) if the ratio of parenchymal to whole kidney volume is known.

To date, the morphological method is the only accepted means of estimating renal parenchymal hemorrhagic volumes and is used as a surrogate for the degree of tissue injury. However, the complexities of kidney preparation and the expertise needed in kidney anatomy and image processing has greatly limited its use by the scientific urological community. On the other hand, investigators at most academic institutions have access to an MRI scanner, and the workflow for the MSNN classifier is relatively easy to perform; thus reducing the time, effort and human error to quantify renal hemorrhagic lesion volumes. These attributes of the MRI method will likely expand the number of investigators able to quantify renal hemorrhagic lesion volumes, allow high throughput screening, and accelerate

improvements in SWL safety and other procedures whose primary renal lesion is hemorrhagic. Conceivably, this MRI method could also be expanded to quantify hemorrhagic lesions *in-vivo* in renal and non-renal organs with some modification of the model.

In summary: A novel MRI data acquisition and workflow system has been developed that rapidly and accurately predicts renal parenchymal lesion volumes derived from whole kidney hemorrhage MRI images. Initially developed to evaluate renal hemorrhagic lesion volumes due to SWL in *ex-vivo* kidneys, the MRI method is currently being adapted for *in vivo* use to provide clinically useful information on the lesion severity, extent and distribution.

Acknowledgments

RKH and PRT contributed equally to the writing of the manuscript (Co-First Authors).

Funding Supported by funds from Renal Imaging Technology Development Program Grant, IIBIS Advanced Technology Grant and Public Health Service Grant P01-DK43881 to RKH and PRT.

References

1. McClain PD, Lange JN, Assimos DG. Optimizing shock wave lithotripsy: A comprehensive review. Rev Urol. 2013; 15:49–60. [PubMed: 24082843]
2. Evan, AP., McAteer, JA. Q-Effects of shock-wave lithotripsy. In: Coe, FL.Favus, MJ.Pak, CYC.Park, JH., Preminger, GM., editors. Kidney Stones: Medical and Surgical Management. Lippincott-Raven Publishers; Philadelphia: 1996. p. 549-570.
3. Evan, AP., Willis, LR. Extracorporeal shock wave lithotripsy: complications. In: Smith, AD.Badlani, GH.Badley, DH., et al., editors. Extracoporeal shock wave lithotripsy. Hamilton, Ontario, Canada: BC Decker; 2007. p. 353-365.Smith's Textbook on Endourology
4. Delvecchio FC, Auge BK, Munver R, et al. Shock wave lithotripsy causes ipsilateral renal injury remote from the focal point: the role of regional vasoconstriction. J Urol. 2003; 169:1526–1529. [PubMed: 12629408]
5. Clark DL, Connors BA, Evan AP, et al. Localization of renal oxidative stress and inflammatory response after lithotripsy. BJU Int. 2009; 103:1562–1568. [PubMed: 19154498]
6. Handa RK, Evan AP. A chronic outcome of shock wave lithotripsy is parenchymal fibrosis. Urol Res. 2010; 38:301–305. [PubMed: 20632169]
7. Handa RK, Johnson CD, Connors BA, et al. Shock wave lithotripsy does not impair renal function in a swine model of metabolic syndrome. J Endourol. 2015; 29:468–473. [PubMed: 25285417]
8. Denburg MR, Jemielita TO, Tasian GE, et al. Assessing the risk of incident hypertension and chronic kidney disease after exposure to shock wave lithotripsy and ureteroscopy. Kidney Int. 2016; 89:185–192. [PubMed: 26509587]
9. Parks JH, Worcester EM, Coe FL, et al. Clinical implications of abundant calcium phosphate in routinely analyzed kidney stones. Kidney Int. 2004; 66:777–785. [PubMed: 15253733]
10. Sarica K, Yencilek F. Prevention of shockwave induced functional and morphological alterations: an overview. Arch Ital Urol Androl. 2008; 80:27–33. [PubMed: 18533622]
11. Lingeman JE, McAteer JA, Gnessin E, et al. Shock wave lithotripsy: advances in technology and technique. Nat Rev Urol. 2009; 6:660–670. [PubMed: 19956196]
12. Blomgren PM, Connors BA, Lingeman JE, et al. Quantitation of shock wave lithotripsy-induced lesion in small and large pig kidneys. Anat Rec. 1997; 249:341–348. [PubMed: 9372167]
13. Ng C-F, Lo AKY, Lee KWM, et al. A prospective, randomized study of the clinical effects of shock wave delivery for unilateral kidney stones: 60 versus 120 shocks per minute. J Urol. 2012; 188:837–842. [PubMed: 22819406]

14. Kardakos IS, Volanis DI, Kalikaki A, et al. Evaluation of neutrophil gelatinase-associated lipocalin, interleukin-18, and cystatin C as molecular markers before and after unilateral shock wave lithotripsy. Urology. 2014; 84:783–788. [PubMed: 25135871]
15. Clark DL, Johnson CD, Blomgren PM, et al. Increased urinary neutrophil gelatinase-associated lipocalin exretion after shock wave lithotripsy in a pig model. J Endourology. 2015; 29(S1):A311. (Abstract).
16. Willis LR, Evan AP, Connors BA, et al. Relationship between kidney size, renal injury, and renal impairment induced by shock wave lithotripsy. J Am Soc Nephrol. 1999; 10:1753–1762. [PubMed: 10446943]
17. Studholme C, Hawkes DJ, Hill DLG. A normalized entropy measure for multimodality image alignment. Proc SPIE Medical Imaging. 1998; 3338:132–143.
18. Kramer, AH., Sangiovanni-Vincentelli, A. Advances in neural information processing systems 1. S.T. David, Morgan Kaufmann Publishers Inc.; 1989. Efficient parallel learning algorithms for neural networks; p. 40-48.

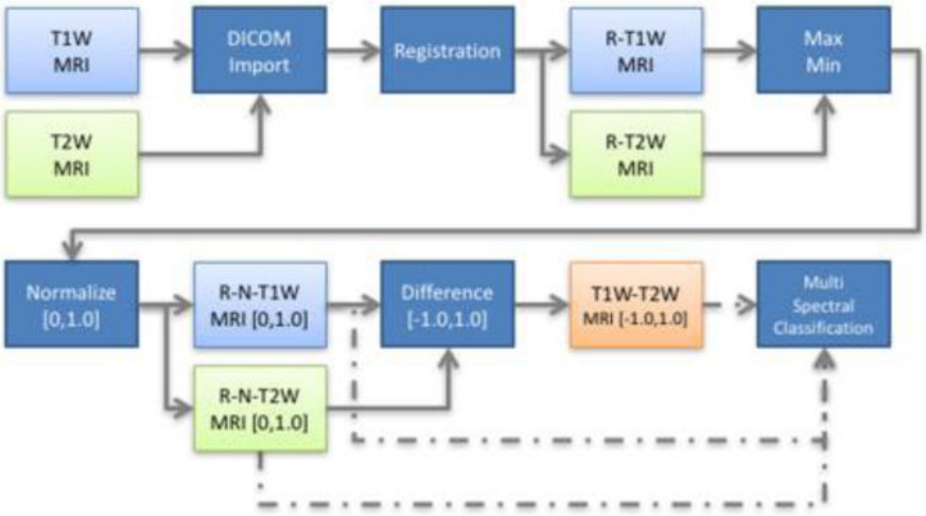

Figure 1.

Image processing workflow for Multi-Spectral Neural Network classification. T1W and T2W images were imported, registered (R), and normalized (N) over the interval [0.0, 1.0], and were subtracted to yield T1W–T2W image which were bound over the interval [−1.0, 1.0]. These registered, normalized, and difference images serve as the model inputs for the Multi-Spectral Neural Network classifier (see Figure 3). In the above diagram, dark blue boxes represent operational steps in the workflow, where solid grey lines indicate the process flow. Light blue, light green, and light orange shapes represent T1W, T2W, and T1W–T2W images, respectively, and dashed lines indicate the images which serve as model inputs.

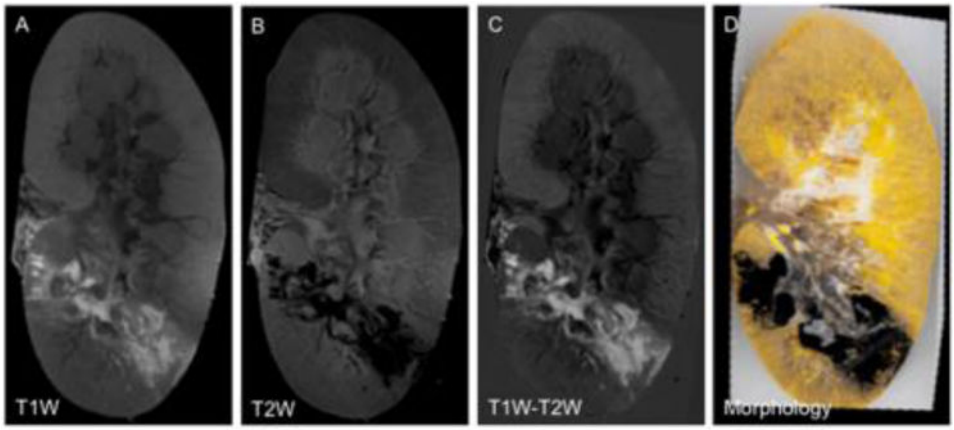

Figure 2.

Representative normalized images of SWL damaged kidneys: (A) T1W, (B) T2W, (C) T1W–T2W, and (D) Embedded coronal morphology image. Images were co-registered using a rigid body normalized entropy mutual information algorithm [17]. Note, in T1W (A) and T1W–T2W (C) images lesions appear bright relative to cortex and medulla, while in T2W (B) and morphology (D) images these same lesions appear darkened.

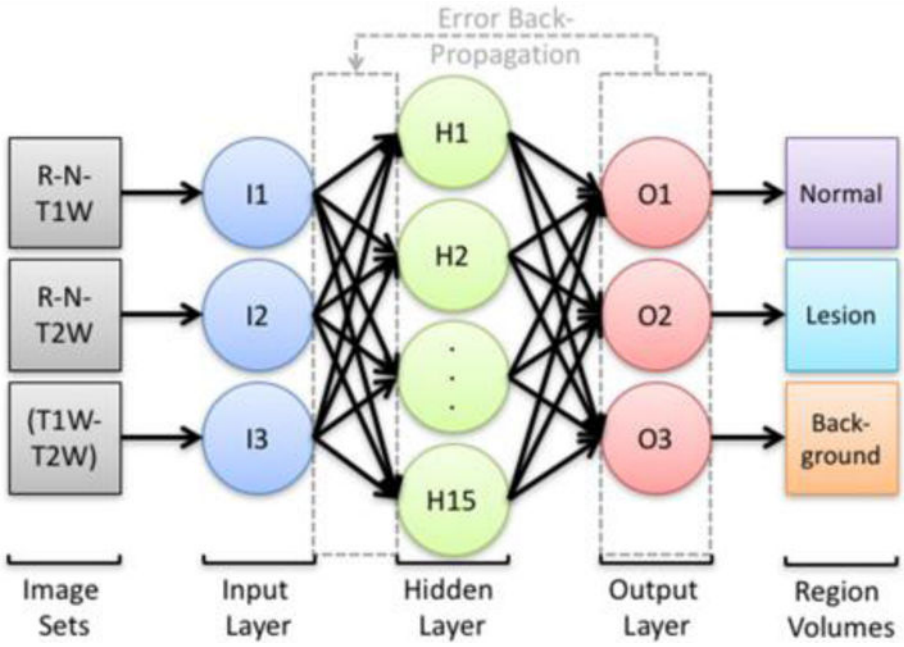

Figure 3.

Multi-Spectral Neural Network Classifier Diagram. Registered (R) and normalized (N) T1W, T2W, T1W–T2W serve as inputs to the model, where nodal weights are applied to the hidden and output layers to yield output voxels which are classified as normal, lesion, or background [18]. In all cases, image datasets used for training were registered and normalized (i.e. [0.0, 1.0]) and modeled to generated nodal weights, which were then applied in an iterative model for all subsequent image datasets. In this system, the following parameters were used: 3 input layers (I1–I3); 15 hidden layers (H1–H15); 3 output layers (O1–O3); $0.1 < \alpha < 0.25$; 200 epochs. The outputs of this model are 3 mask volumes which correspond to the corresponding normal kidney tissue, lesion, and background (i.e. non-tissue).

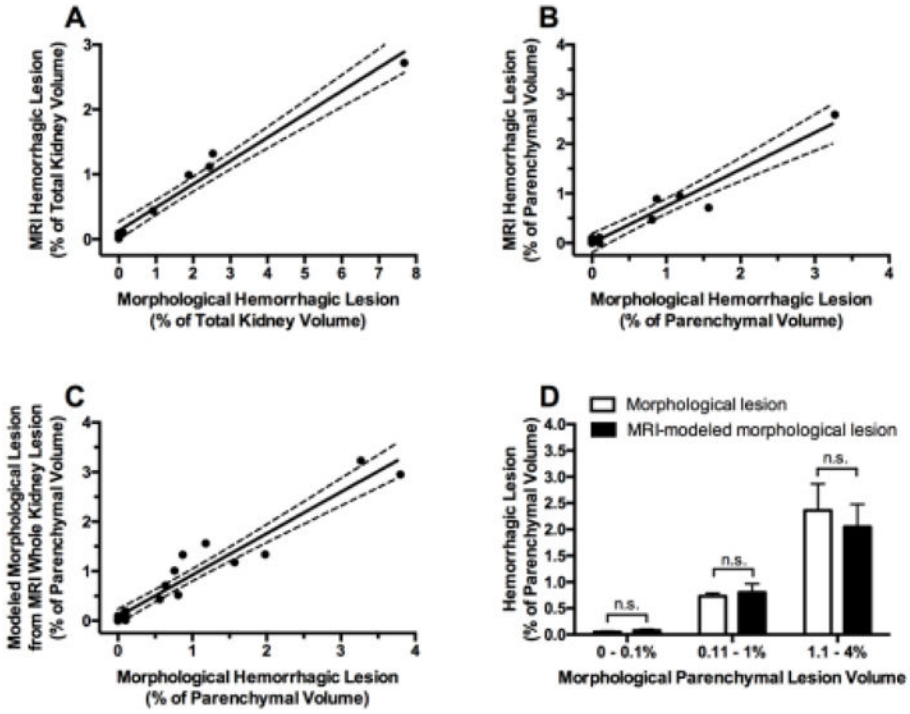

Figure 4.

Comparison of hemorrhagic lesion volumes estimated by morphology vs. MRI using a Multi-Spectral Neural Network model. Dashed lines represent the 95% confidence interval. (A) Total kidney lesion volume, (B) Parenchymal lesion volume, (C) MRI-modeled parenchymal lesion volume, (D) Bar graph of the average MRI-modeled parenchymal lesion and average measured parenchymal lesion when stratified to a range of measured morphological parenchymal lesion volumes. Mean (± standard error of mean) values are shown. n.s. = not significant using a paired Student t-test.